Analyzing Absorption Backgrounds in Single-Walled Carbon Nanotube Spectra

Anton V. Naumov,[†] Saunab Ghosh,[‡] Dmitri A. Tsyboulski,[‡] Sergei M. Bachilo,[‡] and R. Bruce Weisman[‡,*]

[†]Applied Physics Program and [‡]Department of Chemistry, Richard E. Smalley Institute for Nanoscale Science and Technology Rice University, 6100 Main Street, Houston, Texas 77005, United States

ABSTRACT The sources of broad backgrounds in visible—near-IR absorption spectra of single-walled carbon nanotube (SWCNT) dispersions are studied through a series of controlled experiments. Chemical functionalization of nanotube sidewalls generates background absorption while broadening and red-shifting the resonant transitions. Extensive ultrasonic agitation induces a similar background component that may reflect unintended chemical changes to the SWCNTs. No major differences are found between spectral backgrounds in sample fractions with average lengths between 120 and 650 nm. Broad background absorption from amorphous carbon is observed and quantified. Overlapping resonant absorption bands lead to elevated backgrounds from spectral congestion in samples containing many SWCNT structural species. A spectral modeling method is described for separating the background contributions from spectral congestion and other sources. Nanotube aggregation increases congestion backgrounds by broadening the resonant peaks. Essentially no background is seen in sorted pristine samples enriched in a single semiconducting (*n*,*m*) species. By contrast, samples enriched in mixed metallic SWCNTs show broad intrinsic absorption backgrounds far from the resonant transitions. The shape of this metallic background component and its absorptivity coefficient are quantitatively assessed. The results obtained here suggest procedures for preparing SWCNT dispersions with minimal extrinsic background absorptions and for quantifying the remaining intrinsic components. These findings should allow improved characterization of SWCNT samples by absorption spectroscopy.

KEYWORDS: SWCNT · single-walled carbon nanotubes · absorption · spectral background · functionalization · ultrasonication

Single-walled carbon nanotubes (SWCNTs) are artificial nanomaterials whose remarkable properties motivate a wide range of basic and applied research. Current areas of application interest include chemical sensors,[1,2] field emission sources,[3] and medical therapeutic agents.[4−6] Application development is often hampered by impurities in SWCNT bulk samples, which may include residual metal catalysts, multiwall carbon nanotubes, amorphous carbon, and giant fullerenes. Moreover, the SWCNT component is heterogeneous, containing a range of structural species with different diameters, roll-up angles, and electronic characters; a distribution of nanotube lengths; and nanotubes in different states of aggregation and perfection. Sample characterization and purification are therefore essential tasks for SWCNT researchers.

One of the simplest and most widely used tools for SWCNT analysis is absorption spectroscopy in the visible and near-IR. This wavelength range includes the distinct, structure-dependent optical transitions of metallic and semiconducting SWCNTs.[7−9] Underneath these resonant transition peaks is a broad and nearly featureless background. The background has previously been attributed to near-ultraviolet plasmon resonances of nanotubes and carbonaceous impurities.[10,11] Itkis *et al.* devised a sample purity measure based on the ratio of resonant to background absorptions for dispersed samples in which individual (*n*,*m*) peaks are not resolved,[12] and Tan and Resasco have presented a similar "resonance ratio" assessment for samples with resolved peaks.[13] Both assays are based on the idea that at least part of the background absorption arises from sample impurities. Another application of absorption spectroscopy is deducing a sample's (*n*,*m*) distribution by simulating its structured absorption spectrum.[14,15] Such simulations rely on prior knowledge of the (*n*,*m*) species' peak positions.[7,16] Here, in contrast to fluorimetric analysis using background-free SWCNT near-IR emission spectra,[17,18] a correction for the broad background absorption is a critical step in deducing relative magnitudes of specific (*n*,*m*) peaks. A third application in which absorption backgrounds play a central role is estimating the ratio of metallic to semiconducting nanotubes in bulk samples.[19] Knowledge and control of these ratios is particularly important for making SWCNT-based field effect transistors,[20−22] electrical vias,[23] and transparent conductive films.[24,25] Microscopic methods for determining metallic-to-semiconducting ratios have

*Address correspondence to weisman@rice.edu.

Received for review June 16, 2010 and accepted February 8, 2011.

Published online February 22, 2011
10.1021/nn1035922

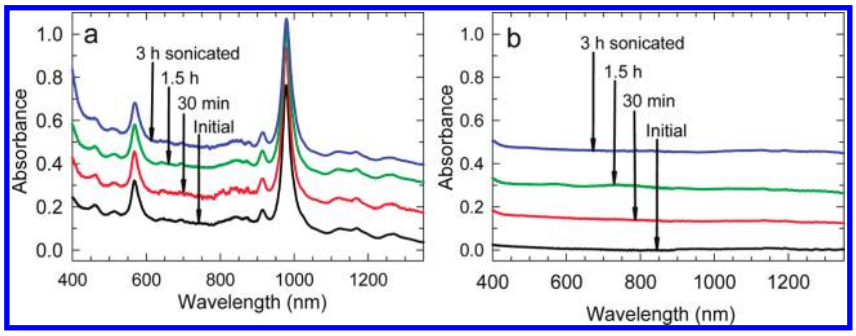

Figure 1. Effects of tip sonication on the absorption spectra of (a) a (6,5)-enriched SWCNT sample suspended in 1% aqueous SDBS and (b) 1% aqueous SDBS without nanotubes. Tip sonication times are 0 min (black curve), 30 min (red curve), 1.5 h (green curve), and 3 h (blue curve).

been developed,[26−28] but they are impractical for routine use. Instead, the relative integrated absorption intensities of bands from metallic and semiconducting species can form the basis of convenient bulk assays.[28,29] However, accurate background subtraction is essential because SWCNT samples typically show broad absorption backgrounds that are more intense than the bands to be quantified. Current suggested approaches rely on modeled absorption backgrounds,[15] and limitations of these models can lead to inaccurate analyses.

We report here an experimental investigation of SWCNT absorption backgrounds. An important part of our approach is to start with samples that have low backgrounds as a result of processing by nonlinear density gradient ultracentrifugation (DGU),[30] and then monitor spectral changes caused by selected perturbations to identify extrinsic and intrinsic background contributions. The effects explored include backgrounds induced by ultrasonication of SWCNTs and surfactants; differences related to nanotube lengths; plasmonic absorption of SWCNTs and carbonaceous impurities; contributions from chemical derivatization; spectral broadening from nanotube bundling; spectral congestion from closely spaced peaks in samples with many (*n*,*m*) species; and absorptions of metallic SWCNT species. We distinguish and quantify several of the factors that can contribute to absorption backgrounds in SWCNT suspensions.

RESULTS AND DISCUSSION

Extrinsic Factors. *Ultrasonication: Surfactant Effects.* A standard step in preparing SWCNT suspensions is dispersion using an ultrasonically agitated immersion tip or bath. To examine the effects of sonication on absorption backgrounds, we began with a SWCNT sample that had been purified and enriched in (6,5) content through nonlinear DGU and suspended in 1% aqueous sodium dodecylbenzenesulfonate (SDBS). The sample initially displayed low relative background absorption, as shown by the bottom trace in Figure 1a. Three hours of bath sonication caused only minor changes in the spectrum. We then applied harsher tip sonication for periods of 30 min to 3 h, while using an ice bath to prevent water evaporation and keep the SWCNT concentration constant. This treatment induced significant systematic increases in absorption background, as shown in Figure 1a, and also a decrease in fluorescence intensity.

The appearance of visible turbidity in the sonicated sample suggested that the observed background elevation might be due to light scattering instead of absorption. To test whether the source of sonication-induced turbidity might be the SDBS surfactant, rather than the SWCNTs, we subjected a solution containing only SDBS to tip sonication for up to 3 h. This processing gave the systematic increases in optical extinction plotted in Figure 1b. However, the sample's spectrum returned to its initial level after mild centrifugation or after standing undisturbed for 12 h under ambient conditions. This implies that extensive tip sonication of SDBS solutions can cause the formation of small particles that are significantly denser than water, presumably through chemical reactions of SDBS during solvent cavitation.

Ultrasonication: SWCNT Effects. To assess the contribution of SWCNTs to the sonication-induced spectral changes seen in Figure 1a, we compared spectra of the sample before tip sonication, after 3 h of tip sonication followed by 12 h of standing, and after 3 h of tip sonication followed by mild centrifugation (Figure 2a). The resonant (6,5) peaks are essentially equal in height, and much of the sonication-induced background has been suppressed by centrifugation. However, there are still significant differences between the initial spectrum and that after sonication and centrifugation, as shown in the subtracted plot of Figure 2b. The additional background rises strongly toward shorter wavelengths, and derivative shapes are evident at the positions of the E_{22} and E_{11} peaks. These derivatives reflect small red shifts of ~3 nm induced by the processing. Raman spectra of the samples (see Figure S1 in Supporting Information) reveal a small decrease in fluorescence but no significant increase in D-band intensity. We attribute the spectral changes to minor sidewall perturbations induced by intense sonication.

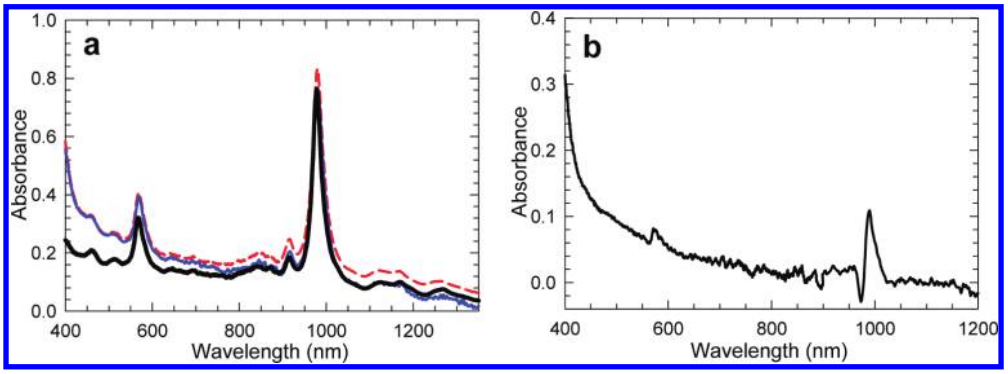

Figure 2. Persistent effects of tip sonication on the absorption spectrum of a (6,5)-enriched SWCNT suspension in aqueous SDBS. (a) Spectra before tip sonication (thick black curve), after 3 h of sonication followed by 12 h of settling (dashed red curve), and after 3 h of sonication followed by mild centrifugation (thin blue curve). (b) Difference spectrum showing net effect of 3 h of sonication and mild centrifugation. Features near 570 and 1000 nm arise from broadening and red shifts of the resonant absorption peaks.

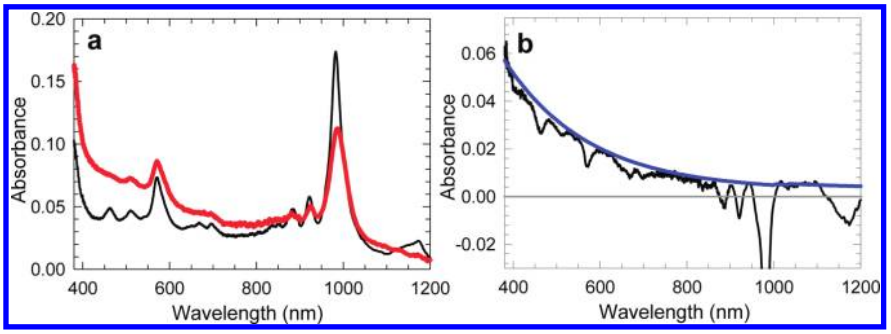

Figure 3. Spectral effects of covalent sidewall reaction. (a) Absorption spectra of a sodium cholate-suspended sample of (6,5)-enriched SWCNTs before (thin black curve) and after (thick red curve) injection of ozone. (b) Difference spectrum of the traces in panel a. Sharp features reflect weakened and broadened resonant peaks in the reacted sample. The smooth blue curve shows an estimate of the broad spectral background induced by the sidewall reaction.

Chemical Functionalization. Typical covalent functionalization of a SWCNT converts carbon atoms from sp^2 to sp^3 hybridization. This removes electrons from the delocalized π-system and introduces localized electronic perturbations that may quench nanotube photoluminescence through nonradiative recombination of mobile excitons.[31] It has also been shown that more extensive covalent functionalization eliminates resonant absorption peaks and leaves a broad, featureless spectrum.[32,33] To monitor the initial spectral changes induced by covalent sidewall functionalization, we exposed a (6,5)-enriched sample of surfactant-suspended SWNCTs to moderate doses of gaseous ozone. (This ozone exposure exceeds that used to induce shifted fluorescence spectra.[34]) Figure 3a shows the sample's absorption spectra before and after this reaction; the difference spectrum is plotted in Figure 3b. The chemical derivatization weakens, broadens, and slightly red-shifts the SWCNT resonant absorption features, particularly the E_{11} peak near 980 nm. It also adds a substantial broad absorption background, which is approximated by the smooth curve in Figure 3b. The shape of this background resembles the one induced by intense sonication. We infer that moderate sidewall derivatization can contribute to SWCNT absorption backgrounds.

Amorphous Carbon Impurities. Amorphous carbon is considered to be a common SWCNT contaminant that may give absorption backgrounds.[12] Its spectrum exhibits strong plasmonic absorption peaking in the near-ultraviolet.[35] To estimate the absorption background contributions from carbonaceous impurities, we prepared aqueous SDBS suspensions of two types of amorphous carbon with particle sizes in the 20−40 nm range (acetylene carbon black and Continental Carbon product N134). Figure 4 panels a and b illustrate the systematic increase of optical extinction with concentration. The spectra from the two types of amorphous carbon clearly have different shapes. However, each can be fit to the three-parameter exponential form $A = a(y_0 + e^{-b\lambda})$ with parameter b fixed for each type. We find that the amplitude parameter a depends linearly on concentration (Figure 4c), with Beer's Law proportionality constants denoted by α_{N134} and α_{Ac}. The differences between fit parameters indicate that background contributions from carbonaceous impurities will vary depending on the form of amorphous carbon. It should nevertheless be possible to estimate a rough upper limit to the amorphous carbon content in a SWCNT sample by fitting the absorption baseline to the functional form given above

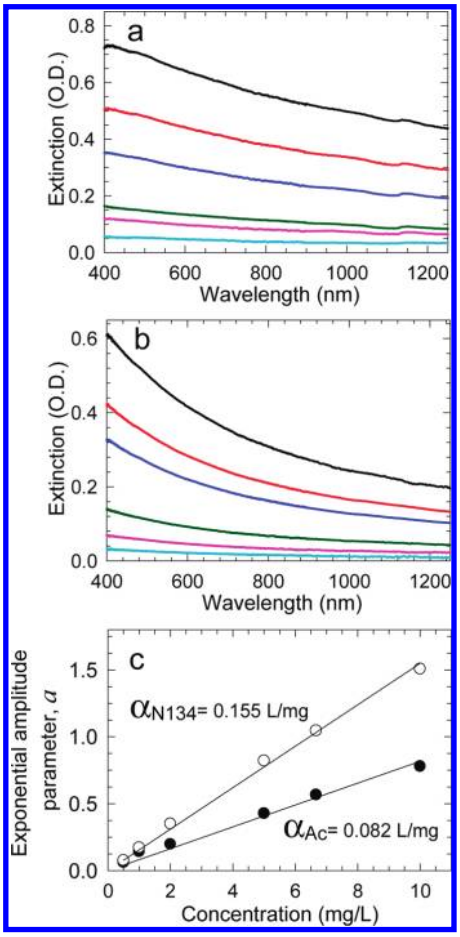

Figure 4. Spectral contributions from amorphous carbon. Extinction spectra (1 cm path length) are shown for different concentrations of two amorphous carbon types: acetylene carbon black (a) and N134 (b). Concentrations (from top to bottom) are 10, 6.7, 5.0, 2.0, 1.0, and 0.5 mg/L. Spectra were fit to the exponential form $A = a(y_0 + e^{-b\lambda})$ with a fixed fit parameter b. For acetylene carbon black, $b = 0.00155$ nm^{-1}; for N134, $b = 0.0030$ nm^{-1}. The linear dependence of fit parameter a on the concentration of amorphous carbon ($a = \alpha \cdot$ concn) is plotted in panel c. α_{N134} and α_{Ac} are the slopes of those linear fits.

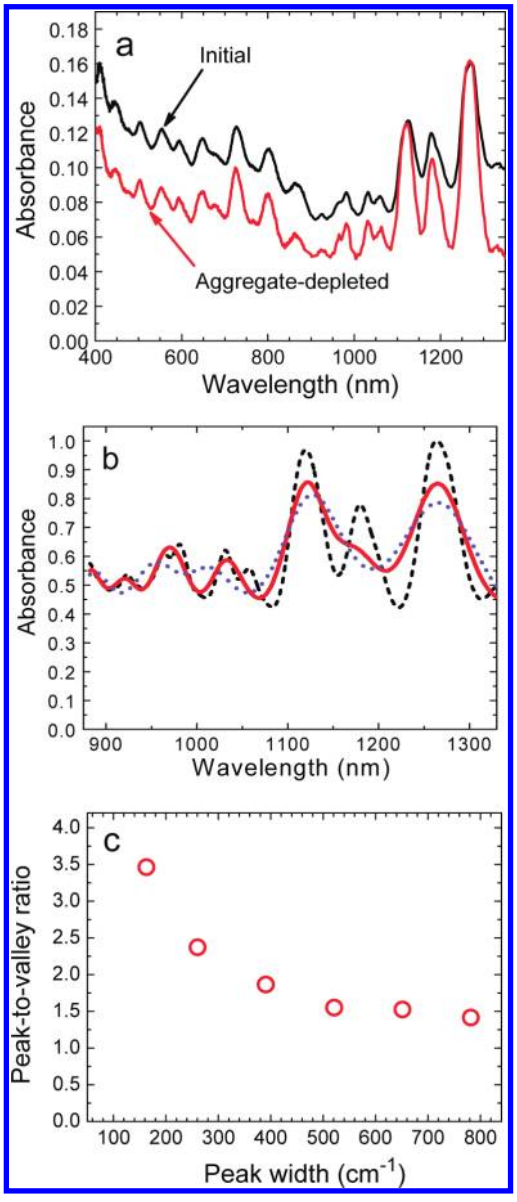

Figure 5. Spectral effects from SWCNT aggregation. (a) Spectra of a SWCNT sample in aqueous sodium deoxycholate before (black) and after (red) DGU processing to remove aggregated nanotubes. The aggregate-depleted spectrum has been scaled to match absorbance values at the 1270 nm peak. (b) Simulated spectra calculated as a sum of individual peaks that are broadened by factors of 2 (solid red curve) and 3 (dotted blue curve), compared to the initial disaggregated spectrum (dashed curve). (c) Dependence of peak-to-valley ratio at the 1264 nm absorption feature on the individual peak widths.

and then dividing the deduced amplitude parameter by a typical α value of 0.1 L/mg.

Aggregation. Another possible source of perturbation in SWCNT absorption spectra is aggregation into nanotube bundles. Aggregation has long been known to broaden and red-shift the resonant absorption peaks,[8] apparently through electronic coupling effects. To examine whether bundling also introduces a broad background, we suspended a polydisperse SWCNT sample in 1% aqueous sodium deoxycholate, centrifuged to remove residual catalyst and carbonaceous impurities, and then compared spectra before and after purification by a DGU procedure that separates out most of the bundles without changing the nanotube length distribution or introducing defects (see Methods). Figure 5a displays absorption spectra of the sample before and after such processing intended to reduce the bundle concentration. The processed sample spectrum shows substantial increases in peak-to-valley ratio, a parameter which has been used to estimate SWCNT sample purity.[12,13,36] In this case, however, the change in peak-to-valley ratio reflects a change in aggregation rather than purity. Nanotube aggregation broadens the resonant absorption peaks and leads to background growth through increased spectral congestion (see following section).

To investigate the effects of individual peak broadening on the overall spectrum, we have simulated the

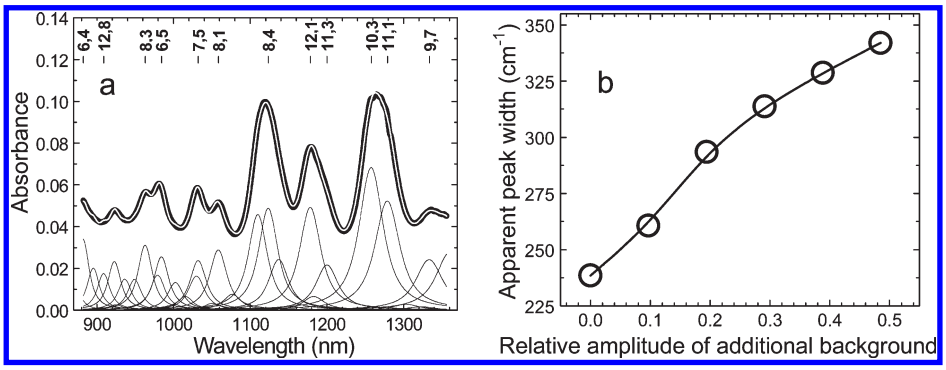

Figure 6. (a) Simulation of a SWCNT near-IR absorption spectrum illustrating spectral congestion. Thick black curve is the measured spectrum of aggregate-depleted SWCNTs in aqueous sodium deoxycholate after subtracting estimated background contribution from metallic SWCNTs. The thin white curve (overlaid with measured spectrum) shows a spectral simulation computed as the sum of individual (*n*,*m*) components, each with a 238 cm^{-1} fwhm and zero background (thin black curves). (b) Dependence of apparent individual peak widths on relative amplitude of added background components. Backgrounds are assumed to have the form $A = ae^{-b\lambda}$ with b = 0.00155 nm^{-1}. The *x*-coordinate represents fit amplitude, *a*, normalized by the intensity of the 1264 nm feature.

measured near-IR absorption spectrum of an aggregate-depleted HiPco sample as a sum of background-free E_{11} peaks from various semiconducting SWCNT species (see following section). When the individual peak widths used in the simulation were increased by up to a factor of 3 to mimic aggregation-induced broadening, the peak-to-valley ratios in the computed spectrum decreased substantially (Figure 5b). Values of these ratios must depend on a sample's (*n*,*m*) distribution and the specific spectral features used in the calculation. For our HiPco spectrum, Figure 5c shows how the ratio found at the 1264 nm absorption peak varies with individual peak width used in simulations. These results indicate that SWCNT aggregation in typical polydisperse samples can cause a factor of 2 decrease in peak-to-valley absorbance ratios.

Intrinsic Effects. *Spectral Congestion.* As illustrated above, absorption backgrounds can appear from spectral congestion: the presence of numerous, closely spaced transitions that overlap over large ranges. Such congestion is expected for SWCNT samples containing relatively large average diameters and broad (*n*,*m*) distributions. To quantify this effect, which is intrinsic to such distributions, we measured the near-IR absorption spectrum of a DGU-processed aggregate-depleted sample similar to the one described in the previous section. We subtracted a broad background contribution from metallic SWCNTs, estimated using the procedure described in the section below on metallic backgrounds and a rough assessment of total SWCNT concentration (see Methods). Using NanoSpectralyzer fitting software, we then simulated the adjusted near-IR spectrum using a parameter set with the positions, widths, and shapes of numerous semiconducting (*n*,*m*) emission peaks, deduced from prior fluorescence analysis of similarly prepared samples in the same surfactant. Minor fitting adjustments were allowed to account for small Stokes shifts between absorption and emission peaks and for some minor peak broadening that can arise from residual nonemissive bundles (which contribute to absorption but not fluorescence spectra). The result is graphed in Figure 6a, where the thin white curve shows the accurate simulation that is the sum of the (*n*,*m*) absorption components plotted below it. Note that although each absorption component in the simulation is assumed to have zero background, their sum gives a spectrum with a substantial background. As this simulation neglects E_{22}^S transitions, which have relatively greater spectral widths than E_{11}^S transitions, we infer that spectral congestion will cause even larger absorption backgrounds at shorter wavelengths in polydisperse SWCNT samples.

We propose a method to distinguish between background components from spectral congestion and other sources in polydisperse samples. It involves a calibration curve that relates apparent peak widths to the background absorptions from other sources. To create the calibration curve, we first modified the simulated spectrum of Figure 6a by adding backgrounds of the form $A = ae^{-\lambda b}$, (chosen to represent contributions from amorphous carbon and metallic nanotubes) with b = 0.00155 nm^{-1} and amplitude parameter a varying from 0 to 0.49 times the peak absorbance at 1264 nm. Then we fit the modified spectrum as a sum of background-free peaks from multiple (*n*,*m*) species, allowing only the common peak width to vary. The peak width needed to fit the modified spectrum increased monotonically with the amplitude of added background, as plotted in Figure 6b. To use this graph, an experimental spectrum would be simulated as a sum of background-free (*n*,*m*) peaks of uniform width (in cm^{-1}). Then Figure 6b is used with the best-fit width value to find the corresponding underlying exponential background that must be present in addition to the spectral congestion background. A properly compensated background will lead to peak widths nearly matching those found in fluorescence analysis of the same sample.

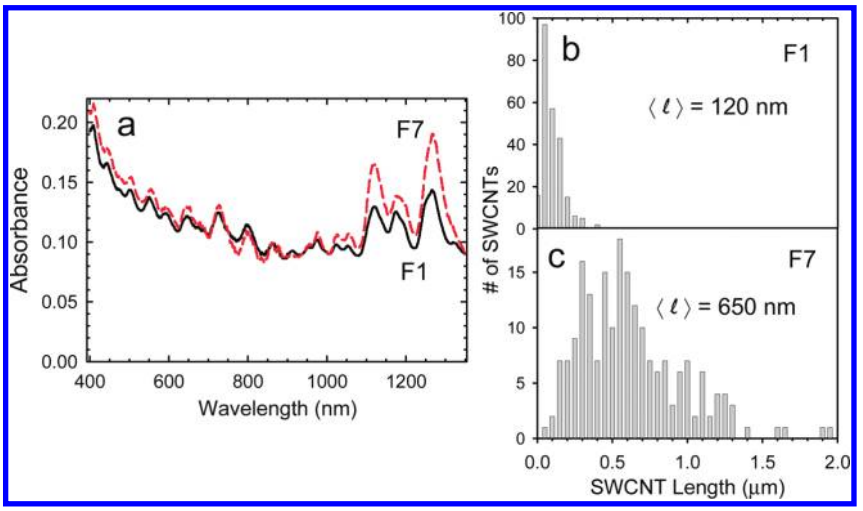

Figure 7. Dependence of absorption spectra on nanotube length. (a) Absorption spectra of two SWCNT fractions: F1 (black solid curve) with average length of 120 nm, and F7 (red dashed curve) with average length of 650 nm. (b),(c) Length histograms of the two fractions obtained by gel electrophoresis. Total numbers of measured nanotubes were 241 and 204, respectively.

SWCNT Length Effects. Nanotube length is another intrinsic property of SWCNTs that might affect absorption backgrounds. If nanotube ends act as defects in the π-electron system, shorter nanotubes would have higher defect densities than longer ones, and therefore possibly more perturbed spectra. We have used gel electrophoresis to separate a SWCNT suspension into fractions of substantially different lengths. Figure 7 panels b and c show AFM length histograms of two of these fractions, which have average lengths of 120 and 650 nm. In Figure 7a we plot the unscaled absorption spectra of the two fractions. We suggest that the lower peak-to-valley ratios, smaller peaks and altered relative peak heights in the short fraction may reflect a combination of minor aggregation and change in diameter distribution from the electrophoresis process.[37] The underlying background absorption appears very similar in both shape and magnitude for the two fractions. We infer that nanotube shortening to ~100 nm does not make a major contribution to observed absorption backgrounds.

Metallic SWCNT Contributions. A final question is whether absorption backgrounds are present in pure, pristine, disaggregated SWCNT samples free of spectral congestion. We used nonlinear DGU to prepare a purified aqueous SWCNT dispersion highly enriched in the (6,5) species and measured its absorption spectrum, shown as the blue curve in Figure 8a. The background here is clearly very low, less than 2% of the E_{11}^S peak height. This demonstrates the absence of intrinsic absorption backgrounds in pure semiconducting SWCNTs.

To investigate whether metallic SWCNTs have similarly low intrinsic backgrounds, we prepared a metallic-enriched (but not (*n*,*m*)-sorted) sample using the same starting material and a comparable dispersion procedure. Impurities and nanotube bundles were removed by DGU. The absorption spectrum of the metallic-enriched sample is shown as the red curve in Figure 8a. Several peaks assigned to resonant transitions of metallic SWCNT species are evident between 500 and 650 nm. The presence of multiple (*n*,*m*) species in this sample may cause some spectral congestion and background elevation below 700 nm, but there is also a significant absorption extending beyond 900 nm that cannot be assigned to tails of the Lorentzian resonant peaks. We suggest that this broad absorption is intrinsic to metallic SWCNTs in the sample. This view is consistent with the dramatic reduction in background absorption found by Nish *et al.* when metallic species were excluded by PFO-assisted dispersion.[38] One possible interpretation is that the broad absorption is the tail of the π-plasmon resonance,[39] which may be more intense (relative to E_{11} transitions) in metallic than in semiconducting SWCNTs. Another possible assignment is to E_{00}^M or E_{01}^M transitions, which would appear at longer wavelengths than E_{11}^M and have no counterpart in semiconducting nanotubes.[40] Although theory predicts such transitions to be symmetry-forbidden or weakened by depolarization effects,[40] we speculate that they might be observable in chiral metallic SWCNTs, in which axial symmetry lower than for armchair and zigzag species[41] might lead to subbands of mixed angular momentum character. Regardless of detailed assignment, our experimental results indicate that intrinsic absorption backgrounds are present in some metallic but not in semiconducting SWCNTs.

To quantify these backgrounds with respect to metallic SWCNT concentration, we have used a sample of solid metallic-enriched SWCNTs to prepare three aqueous suspensions of known concentration. Absorption spectra of these suspensions (Figure 8b) show a single unresolved metallic peak at a longer wavelength than the ones in Figure 8a, reflecting the larger average diameter of this SWCNT sample. As in the spectrum of Figure 8a, all of these spectra show absorption backgrounds tailing into

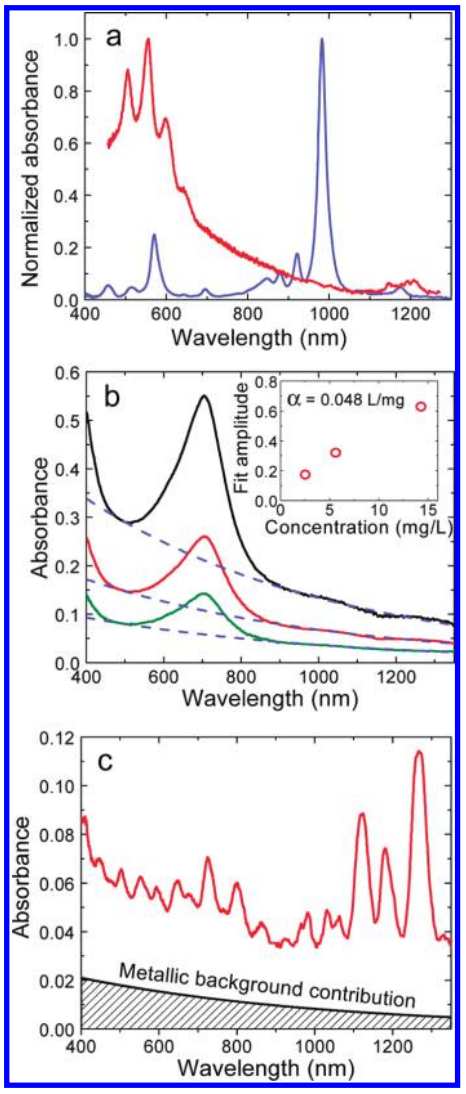

Figure 8. Absorption spectra of DGU-processed SWCNT samples. (a) Highly (6,5)-enriched semiconducting sample (blue curve) and a metallic-enriched sample from the same growth batch (red curve). The weak features near 1200 nm are uncompensated solvent absorptions. (b) Absorption spectra of larger diameter metallic-enriched SWCNTs at concentrations of 2.5, 5.6, and 14.3 mg/L (green, red, and black curves, respectively). Backgrounds are represented by the blue dashed curves of the form $A = ae^{-b\lambda}$ with b = 0.00155 nm^{-1}. Inset shows the dependence of fit parameter a on the SWCNT concentration. The deduced slope is 0.048 L/mg. (c) Absorption spectrum of an aggregate-depleted SWCNT sample (red curve) and the estimated metallic background contribution (see text).

near-infrared. To assess the concentration dependence of the backgrounds, we fitted them with a single-parameter exponential function, $A = ae^{-b\lambda}$ with fixed b = 0.00155 nm^{-1}, and observed a nearly linear correlation between amplitude parameter a and SWCNT concentration (inset in Figure 8b). The y-intercept of the correlation is small but nonzero, likely because of surfactant damage during sonication. We find a slope, α, of 0.048 L mg^{-1} based on the first two points (complete sample dispersion was not achieved in the highest concentration sample).

This value of α allows estimation of the contribution of metallic SWCNTs to the absorption background of polydisperse samples. If the total SWCNT mass concentration of a sample is known, its metallic concentration can be found using experimental values of metallic percentages reported for nanotubes from a variety of sources.[42] The deduced metallic SWCNT concentration is then multiplied by α to obtain parameter a in the expression $A = ae^{-b\lambda}$ that represents the background contribution of the metallic nanotubes.

Suggested Procedure for Estimating and Decreasing Absorption Backgrounds. We can use the findings described in the sections above to minimize complications caused by absorption backgrounds. The first step is careful sample processing. A solid SWCNT sample should be dispersed in a surfactant known to provide good individualization, using the minimum ultrasonic agitation needed for complete dispersion (so as to avoid sonication-induced background contributions). The DGU procedure used for our aggregation studies (see Methods) will then remove most nanotube bundles as well as residual catalyst and amorphous carbon impurities. One can monitor the relative extent of disaggregation by measuring absorption peak-to-valley ratios (as in Figure 5).

Following this processing, the absorption spectrum of the purified sample is analyzed for spectral congestion and metallic background components. Spectral congestion is evaluated using the procedure described in the corresponding section above. The apparent peak widths found from that fitting procedure are used to estimate the background elevation from other sources (see Figure 6b). Assuming that there is no significant functionalization of the sample, this remaining background is attributed to metallic SWCNTs (Figure 8c). To estimate the concentration of these metallic SWCNTs, divide the exponential fit amplitude, a, by the value of α shown in Figure 8b. If the total SWCNT mass concentration is known for the sample, then this procedure allows estimation of the semiconducting-to-metallic ratio.

CONCLUSIONS

We have investigated and quantitatively assessed a number of possible sources of absorption background in dispersed SWCNT samples. Operationally, exposure to extended intense ultrasonication can give backgrounds attributed to scattering from particulates formed during surfactant agitation. Strong sonication is also observed to give a persistent spectral background component that may arise from unintended nanotube chemical reactions or damage but appears unlikely to result from simple shortening of nanotubes down to ~100 nm. Sidewall chemical functionalization broadens resonant components and adds a spectral background that increases toward shorter wavelengths. An additional absorption background is induced by carbonaceous impurities, and absorptivity

coefficients are reported for this background contribution. Well-dispersed pristine SWCNT samples enriched in a specific semiconducting (*n*,*m*) species display nearly background-free absorption spectra. However, similar samples containing a wide range of semiconducting species show elevated backgrounds from spectral congestion due to overlapping resonant absorption peaks. A spectral simulation fitting routine distinguishes spectral congestion from other background components. We also find that spectral congestion backgrounds are increased by nanotube aggregation. The relative extent of nanotube aggregation may be monitored using peak-to valley ratios in the absorption spectrum. In contrast to their semiconducting counterparts, mixtures of metallic SWCNTs apparently have intrinsic broad absorption backgrounds, whose absorptivity coefficient has been determined.

Our results suggest that a combination of sample processing and analysis methods can minimize the absorption backgrounds of SWCNT samples and identify the remaining contributions from spectral congestion and metallic SWCNTs. This procedure allows one to find relative magnitudes of (*n*,*m*)-specific E_{11} absorption bands. If the sample concentration is known, it is also possible to estimate the semiconducting-to-metallic ratio in the SWCNT sample. We believe that our findings will increase the value of absorption spectroscopy as a tool for analyzing SWCNT sample purity and content.

METHODS

Sample Preparation and Processing. All SWCNT suspensions (except for the metallic-enriched sample from NanoIntegris) were prepared using HiPco product (batch 188.4) from the Rice University reactor. Studies of ultrasonication effects were performed on (6,5)-enriched SWCNT suspensions prepared according to the nonlinear DGU protocol reported recently.[30] We changed the surfactant from aqueous sodium cholate (used in DGU) to 1% SDBS by filtering through a Nanosep 10K centrifugal filter, washing the nanotubes to remove sodium cholate, and resuspending them in 1% aqueous SDBS.

For experiments involving up to 3 h of bath ultrasonication, we used a Sharpertek model Stamina XP (4.5 L) sonicator. Tip sonication experiments were performed in an ice bath on sample volumes of approximately 1.5 mL using a Misonix model XL-2000 at powers of 4−5 W. Sonication-induced turbidity was reduced by centrifuging at 2800 *g* for 5 min or by passive sedimentation under ambient conditions for 12 h.

Absorption backgrounds were studied for two amorphous carbon sources: 99.99% pure acetylene carbon black (Strem Chemicals, CAS no. 7440-44-0) and N134 (Continental Carbon), with particle sizes of 42 nm and 20−40 nm, respectively. Each of these materials was ultrasonically suspended in 1% aqueous SDBS to create six suspensions with concentrations of 10, 6.7, 5, 2, 1, and 0.5 mg/L. Sonication was preformed in an ice bath to prevent concentration changes from solvent evaporation.

The effects of SWCNT functionalization on absorption background were investigated by stepwise injection of up to 290 μg of gaseous ozone in O_2 (from an Ozone Services model GE60 generator) into 80 μL of (6,5)-enriched SWCNTs in 1% aqueous sodium cholate.

For assessing spectral changes from aggregation, we compared a dispersed SWCNT sample that had been mildly centrifuged to remove carbonaceous and catalyst impurities with another sample also subjected to rigorous DGU processing to further separate individual nanotubes from bundles.[43] The DGU density gradient was prepared by discrete layering of premixed aliquots of water and iodixanol of variable density (1.5 mL of 1.32 g/cm^3, 1.0 mL of 1.25 g/cm^3, 0.5 mL of 1.20 g/cm^3, 0.5 mL of 1.15 g/cm^3, 0.5 mL of 1.10 g/cm^3, 0.5 mL of 1.05 g/cm^3). The layered centrifuge tube was capped and tilted at an angle of 10° for 30 min. Then 0.5 mL of previously prepared SWCNT suspension in sodium cholate was added and the tube was centrifuged for 12 h at 268000*g*. The resulting suspension separated into two distinct fractions with the upper one containing mostly individual SWCNTs. This aggregate-depleted fraction was then used for studies of spectral congestion and aggregation effects.

To investigate SWCNT length effects, SWCNT suspensions in 1% aqueous sodium deoxycholate were initially prepared using sequential bath and tip sonication followed by the aggregate-removing DGU protocol described above. The sample was then length fractionated by electrophoresis in a 5% agarose gel using a procedure similar to that of Heller *et al.*[37] To determine nanotube length distributions, fractions were drop-cast onto silicon substrates, washed, and annealed at 450 °C to decrease the amount of residual surfactant. After this treatment, we compiled length histograms for each fraction by analyzing images taken with a Veeco Multimode 3A atomic force microscope.

Absorption background contributions from metallic SWCNTs were studied using nanotubes from two different sources. A sample of (6,5)-enriched SWCNTs in aqueous sodium cholate was prepared from HiPco batch 188.4 by nonlinear DGU, as described previously.[30] SWCNTs from the same batch were dispersed in a sodium cholate/SDS mixture and DGU-processed for metallic enrichment.[43] The metallic-enriched fraction was dialyzed against 1% aqueous sodium cholate in a 10 kD dialysis cassette. The concentration dependence of SWCNT metallic absorption backgrounds was assessed using solutions prepared from a solid 99% metallic-enriched SWCNT sample (NanoIntegris). Weighed portions of this sample were dispersed in known volumes of 1% sodium cholate solution by 20 min tip sonication at 4 W in an ice bath to yield SWCNT mass concentrations of 2.5, 5.6, and 14.3 mg/L.

For the purpose of estimating metallic contributions when modeling spectral congestion, a weighed amount of HiPco SWCNTs was dispersed in a known volume of DMF by 20 min of tip sonication at 4 W. The absorption spectrum of the resulting suspensions was measured, and DMF was then evaporated on a hot plate to constant sample weight. The absorbance per unit mass found for the sample was used to estimate the concentration of the aggregate-depleted sample used in spectral congestion modeling.

Apparatus. Visible−near-IR absorption and Raman spectra (740 nm excitation) were measured using a model NS2 NanoSpectralyzer (Applied NanoFluorescence, LLC).

Acknowledgment. This research was supported by grants from the National Science Foundation (CHE-0809020) and the Welch Foundation (C-0807). We thank M. Johnson of Continental Carbon for providing carbon black samples.

Supporting Information Available: Raman spectra of the (6,5)-enriched SWCNT sample in aqueous SDBS after 30 min to 3 h of tip sonication. This material is available free of charge *via* the Internet at http://pubs.acs.org.

REFERENCES AND NOTES

1. Kong, J.; Franklin, N. R.; Zhou, C. W.; Chapline, M. G.; Peng, S.; Cho, K. J.; Dai, H. J. Nanotube Molecular Wires as Chemical Sensors. *Science* **2000,** *287*, 622–625.

2. Kong, J.; Chapline, M. G.; Dai, H. J. Functionalized Carbon Nanotubes for Molecular Hydrogen Sensors. *Adv. Mater.* **2001,** *13*, 1384–1386.
3. Lim, S. C.; Lee, K.; Lee, I. H.; Lee, Y. H. Field Emission and Application of Carbon Nanotubes. *Nano* **2007,** *2*, 69–89.
4. Kam, N. W. S.; O'Connell, M. J.; Wisdom, J. A.; Dai, H. Carbon Nanotubes as Multifunctional Biological Transporters and Near-Infrared Agents for Selective Cancer Cell Destruction. *Proc. Natl. Acad. Sci. U.S.A.* **2005,** *102*, 11600–11605.
5. Bhirde, A. A.; Patel, V.; Gavard, J.; Zhang, G. F.; Sousa, A. A.; Masedunskas, A.; Leapman, R. D.; Weigert, R.; Gutkind, J. S.; Rusling, J. F. Targeted Killing of Cancer Cells *in Vivo* and *in Vitro* With EGF-Directed Carbon Nanotube-Based Drug Delivery. *ACS Nano* **2009,** *3*, 307–316.
6. Bartholomeusz, G.; Cherukuri, P.; Kingston, J.; Cognet, L.; Lemos, R.; Leeuw, T. K.; Gumbiner-Russo, L.; Weisman, R. B.; Powis, G. *In Vivo* Therapeutic Silencing of Hypoxia-Inducible Factor 1 Alpha (HIF-1α) Using Single-Walled Carbon Nanotubes Noncovalently Coated with SiRNA. *Nano Res.* **2009,** *2*, 279–291.
7. Bachilo, S. M.; Strano, M. S.; Kittrell, C.; Hauge, R. H.; Smalley, R. E.; Weisman, R. B. Structure-Assigned Optical Spectra of Single-Walled Carbon Nanotubes. *Science* **2002,** *298*, 2361–2366.
8. O'Connell, M. J.; Bachilo, S. M.; Huffman, C. B.; Moore, V.; Strano, M. S.; Haroz, E.; Rialon, K.; Boul, P. J.; Noon, W. H.; Kittrell, C.; *et al*. Band-Gap Fluorescence From Individual Single-Walled Carbon Nanotubes. *Science* **2002,** *297*, 593–596.
9. Strano, M. S.; Doorn, S. K.; Haroz, E.; Kittrell, C.; Hauge, R. H.; Smalley, R. E. Assignment of (*n*,*m*) Raman and Optical Features of Metallic Single-Walled Carbon Nanotubes. *Nano Lett.* **2003,** *3*, 1091–1096.
10. Kataura, H.; Kumazawa, Y.; Maniwa, Y.; Umezu, I.; Suzuki, S.; Ohtsuka, Y.; Achiba, Y. Optical Properties of Single-Wall Carbon Nanotubes. *Synth. Met.* **1999,** *103*, 2555–2558.
11. Murakami, Y.; Einarsson, E.; Edamura, T.; Maruyama, S. Polarization Dependence of the Optical Absorption of Single-Walled Carbon Nanotubes. *Phys. Rev. Lett.* **2005,** *94*, 087402-1–087402-4.
12. Itkis, M. E.; Perea, D. E.; Niyogi, S.; Rickard, S. M.; Hamon, M. A.; Zhao, B.; Haddon, R. C. Purity Evaluation of As-Prepared Single-Walled Carbon Nanotube Soot by Use of Solution-Phase Near-IR Spectroscopy. *Nano Lett.* **2003,** *3*, 309–314.
13. Tan, Y.; Resasco, D. E. Dispersion of Single-Walled Carbon Nanotubes of Narrow Diameter Distribution. *J. Phys. Chem. B* **2005,** *109*, 14454–14460.
14. Luo, Z.; Pfefferle, L. D.; Haller, G. L.; Papadimitrakopoulos, F. (*n*,*m*) Abundance Evaluation of Single-Walled Carbon Nanotubes by Fluorescence and Absorption Spectroscopy. *J. Am. Chem. Soc.* **2006,** *128*, 15511–15516.
15. Nair, N.; Usrey, M. L.; Kim, W.; Braatz, R. D.; Strano, M. S. Estimation of the (*n*,*m*) Concentration Distribution of Single-Walled Carbon Nanotubes From Photoabsorption Spectra. *Anal. Chem.* **2006,** *78*, 7689–7696.
16. Weisman, R. B.; Bachilo, S. M. Dependence of Optical Transition Energies on Structure for Single-Walled Carbon Nanotubes in Aqueous Suspension: An Empirical Kataura Plot. *Nano Lett.* **2003,** *3*, 1235–1238.
17. Bachilo, S. M.; Balzano, L.; Herrera, J. E.; Pompeo, F.; Resasco, D. E.; Weisman, R. B. Narrow (*n*,*m*)-Distribution of Single-Walled Carbon Nanotubes Grown Using a Solid Supported Catalyst. *J. Am. Chem. Soc.* **2003,** *125*, 11186–11187.
18. Weisman, R. B. Fluorimetric Characterization of Single-Walled Carbon Nanotubes. *Anal. Bioanal. Chem.* **2010,** *396*, 1015–1023.
19. Miyata, Y.; Yanagi, K.; Maniwa, Y.; Kataura, H. Optical Evaluation of the Metal-to-Semiconductor Ratio of Single-Wall Carbon Nanotubes. *J. Phys. Chem. C* **2008,** *112*, 13187–13191.
20. Avouris, P.; Radosavljevic, M.; Wind, S. J. Carbon Nanotube Electronics and Optoelectronics, In *Applied Physics of Carbon Nanotubes*; Rotkin, S. V., Subramoney, S., Eds.; Springer: Berlin, 2005; pp 227−251.
21. Martel, R.; Schmidt, T.; Shea, H. R.; Hertel, T.; Avouris, P. Single- and Multi-Wall Carbon Nanotube Field-Effect Transistors. *Appl. Phys. Lett.* **1998,** *73*, 2447–2449.
22. Tans, S. J.; Verschueren, A. R. M.; Dekker, C. Room-Temperature Transistor Based on a Single Carbon Nanotube. *Nature* **1998,** *393*, 49–52.
23. Yao, Z.; Kane, C. L.; Dekker, C. High-Field Electrical Transport in Single-Wall Carbon Nanotubes. *Phys. Rev. Lett.* **2000,** *84*, 2941–2944.
24. Wu, Z. C.; Chen, Z. H.; Du, X.; Logan, J. M.; Sippel, J.; Nikolou, M.; Kamaras, K.; Reynolds, J. R.; Tanner, D. B.; Hebard, A. F.; *et al*. Transparent, Conductive Carbon Nanotube Films. *Science* **2004,** *305*, 1273–1276.
25. Yu, X.; Rajamani, R.; Stelson, K. A.; Cui, T. Carbon Nanotube Based Transparent Conductive Thin Films. *J. Nanosci. Nanotechnol.* **2006,** *6*, 1939–1944.
26. Lu, W.; Xiong, Y.; Hassanien, A.; Zhao, W.; Zheng, M.; Chen, L. A Scanning Probe Microscopy Based Assay for Single-Walled Carbon Nanotube Metallicity. *Nano Lett.* **2009,** *9*, 1668–1672.
27. Naumov, A. V.; Kuznetsov, O. A.; Harutyunyan, A. R.; Green, A. A.; Hersam, M. C.; Resasco, D. E.; Nikolaev, P. N.; Weisman, R. B. Quantifying the Semiconducting Fraction in Single-Walled Carbon Nanotube Samples Through Comparative Atomic Force and Photoluminescence Microscopies. *Nano Lett.* **2009,** *9*, 3203–3208.
28. Kim, W. J.; Lee, C. Y.; O'Brien, K. P.; Plombon, J. J.; Blackwell, J. M.; Strano, M. S. Connecting Single Molecule Electrical Measurements to Ensemble Spectroscopic Properties for Quantification of Single-Walled Carbon Nanotube Separation. *J. Am. Chem. Soc.* **2009,** *131*, 3128–3129.
29. Blackburn, J. L.; Barnes, T. M.; Beard, M. C.; Kim, Y. H.; Tenent, R. C.; McDonald, T. J.; To, B.; Coutts, T. J.; Heben, M. J. Transparent Conductive Single-Walled Carbon Nanotube Networks With Precisely Tunable Ratios of Semiconducting and Metallic Nanotubes. *ACS Nano* **2008,** *2*, 1266–1274.
30. Ghosh, S.; Bachilo, S. M.; Weisman, R. B. Advanced Sorting of Single-Walled Carbon Nanotubes by Nonlinear Density-Gradient Ultracentrifugation. *Nat. Nanotechnol.* **2010,** *5*, 443–450.
31. Cognet, L.; Tsyboulski, D.; Rocha, J.-D. R.; Doyle, C. D.; Tour, J. M.; Weisman, R. B. Stepwise Quenching of Exciton Fluorescence in Carbon Nanotubes by Single-Molecule Reactions. *Science* **2007,** *316*, 1465–1468.
32. Banerjee, S.; Wong, S. S. Rational Sidewall Functionalization and Purification of Single-Walled Carbon Nanotubes by Solution-Phase Ozonolysis. *J. Phys. Chem. B* **2002,** *106*, 12144–12151.
33. Dyke, C. A.; Tour, J. M. Solvent-Free Functionalization of Carbon Nanotubes. *J. Am. Chem. Soc.* **2003,** *125*, 1156–1157.
34. Ghosh, S.; Bachilo, S. M.; Simonette, R. A.; Beckingham, K. M.; Weisman, R. B. Oxygen Doping Modifies Near-Infrared Band Gaps in Fluorescent Single-Walled Carbon Nanotubes. *Science* **2010,** *330*, 1656–1659.
35. Day, K. L.; Huffman, D. R. Measured Extinction Efficiency of Graphite Smoke in Region 1200−6000 A. *Nat. Phys. Sci.* **1973,** *243*, 50–51.
36. Landi, B. J.; Ruf, H. J.; Evans, C. M.; Cress, C. D.; Raffaelle, R. P. Purity Assessment of Single-Wall Carbon Nanotubes, Using Optical Absorption Spectroscopy. *J. Phys. Chem. B* **2005,** *109*, 9952–9965.
37. Heller, D. A.; Mayrhofer, R. M.; Baik, S.; Grinkova, Y. V.; Usrey, M. L.; Strano, M. S. Concomitant Length and Diameter Separation of Single-Walled Carbon Nanotubes. *J. Am. Chem. Soc.* **2004,** *126*, 14567–14573.
38. Nish, A.; Hwang, J. Y.; Doig, J.; Nicholas, R. J. Highly Selective Dispersion of Singlewalled Carbon Nanotubes Using Aromatic Polymers. *Nat. Nanotechnol.* **2007,** *2*, 640–646.
39. Pichler, Th.; Knupfer, M.; Golden, M. S.; Fink, J.; Rinzler, A.; Smalley, R. E. Localized and Delocalized Electronic States in Single-Wall Carbon Nanotubes. *Phys. Rev. Lett.* **1998,** *80*, 4729–4732.
40. Ando, T. Theory of Electronic States and Transport in Carbon Nanotubes. *J. Phys. Soc. Jpn.* **2005,** *74*, 777–817.

41. Damnjanovic, M.; Milosevic, I.; Vukovic, T.; Sredanovic, R. Full Symmetry, Optical Activity, and Potentials of Single-Wall and Multiwall Nanotubes. *Phys. Rev. B* **1999,** *60*, 2728–2739.
42. Naumov, A. V.; Kuznetsov, O. A.; Harutyunyan, A. R.; Green, A. A.; Hersam, M. C.; Resasco, D. E.; Nikolaev, P. N.; Weisman, R. B. Quantifying the Semiconducting Fraction in Single-Walled Carbon Nanotube Samples Through Comparative Atomic Force and Photoluminescence Microscopies. *Nano Lett.* **2009,** *9*, 3203–3208.
43. Arnold, M. S.; Green, A. A.; Hulvat, J. F.; Stupp, S. I.; Hersam, M. C. Sorting Carbon Nanotubes by Electronic Structure Using Density Differentiation. *Nat. Nanotechnol.* **2006,** *1*, 60–65.